International Journal of Nanomedicine

Dovepress
open access to scientific and medical research

Open Access Full Text Article

ORIGINAL RESEARCH

Development and evaluation of thymoquinone-encapsulated chitosan nanoparticles for nose-to-brain targeting: a pharmacoscintigraphic study

This article was published in the following Dove Press journal:
International Journal of Nanomedicine
8 November 2012
Number of times this article has been viewed

Sanjar Alam[1]
Zeenat I Khan[1]
Gulam Mustafa[1]
Manish Kumar[2]
Fakhrul Islam[3]
Aseem Bhatnagar[4]
Farhan J Ahmad[1]

[1]Department of Pharmaceutics, Faculty of Pharmacy, Jamia Hamdard, Hamdard Nagar, New Delhi, India; [2]Advanced Instrumentation Research Facility, Jawaharlal Nehru University, New Delhi, India; [3]Department of Medical Elementology and Toxicology, Neurotoxicology Laboratory, Jamia Hamdard, Hamdard Nagar, New Delhi, India; [4]Government of India, Ministry of Defence, Institute of Nuclear Medicine and Allied Sciences, Brig SK Mazumdar Marg, Delhi, India

Abstract: Chitosan (CS) nanoparticles of thymoquinone (TQ) were prepared by the ionic gelation method and are characterized on the basis of surface morphology, in vitro or ex vivo release, dynamic light scattering, and X-ray diffractometry (XRD) studies. Dynamic laser light scattering and transmission electron microscopy confirmed the particle diameter was between 150 to 200 nm. The results showed that the particle size of the formulation was significantly affected by the drug:CS ratio, whereas it was least significantly affected by the tripolyphosphate:CS ratio. The entrapment efficiency and loading capacity of TQ was found to be 63.3% ± 3.5% and 31.23% ± 3.14%, respectively. The drug-entrapment efficiency and drug-loading capacity of the nanoparticles appears to be inversely proportional to the drug:CS ratio. An XRD study proves that TQ dispersed in the nanoparticles changes its form from crystalline to amorphous. This was further confirmed by differential scanning calorimetry thermography. The flat thermogram of the nanoparticle data indicated that TQ formed a molecular dispersion within the nanoparticles. Optimized nanoparticles were evaluated further with the help of scintigraphy imaging, which ascertains the uptake of drug into the brain. Based on maximum concentration, time-to-maximum concentration, area-under-curve over 24 hours, and elimination rate constant, intranasal TQ-loaded nanoparticles (TQ-NP1) proved more effective in brain targeting compared to intravenous and intranasal TQ solution. The high drug-targeting potential and efficiency demonstrates the significant role of the mucoadhesive properties of TQ-NP1.

Keywords: thymoquinone, chitosan, nanoparticles, nose-to-brain targeting, gamma scintigraphy

Introduction

Alzheimer's disease (AD) is the most common form of progressive neurodegenerative disorder and primarily affects the elderly population (50%–60% of the >65-year-old age group).[1] More than 18 million of the global population currently suffers from AD and this is expected to double by 2025. AD is a major medical and social problem for developing societies. The etiology of AD involves cognitive dysfunction, primarily memory loss,[2,3] and in later stages it causes language deficits, depression, and behavioral problems including agitation, mood disturbances, and psychosis.[4,5]

Moreover, senile plaques, neurofibrillary tangles, oxidative stress, inflammatory processes, and neurotransmitter disturbances are common diagnostic features found in the brain of an AD patient. Many promising agents have failed in clinical trials because of their therapeutic limitations in providing symptomatic relief from cognitive deficits. An agent that not only improves cognitive functions, but also blocks neuronal loss in the brain, is urgently needed.[6] Alternatively, the use of medicinal plants has been

Correspondence: Farhan J Ahmad
Department of Pharmaceutics, Faculty of Pharmacy, Jamia Hamdard, Hamdard Nagar, New Delhi, India 110062
Tel +91 98 9167 4226
Email sanjaralam10@gmail.com

another new therapeutic approach in the treatment of AD.[7] Most herbal drugs, especially those with a hydrophobic nature, although possessing excellent potential, fail in clinical trials because of a lack of safety or poor efficacy. Although natural products have served as sources for the majority of drugs, poor oral bioavailability has hindered their development.[7] In traditional and folk medicines, herbal drugs have been used extensively to enhance cognition and to alleviate other symptoms associated with AD.[8] This approach has been used in various practices of traditional medicine, including Ayurveda and Unani, where herbal medication is frequently prescribed. An ethnopharmacologic approach for the treatment of AD is expected to be useful in providing leads to identify plants and potential new drugs.

Recently, thymoquinone (TQ) a major active lipophilic component of *Nigella Sativa* (Ranunculaceae) was reported to have many pharmacological qualities such as its immunomodulation, anticancer, anti-inflammatory, antiasthmatic, and antioxidant effects. In many reports, the antioxidant and anti-inflammatory effects showed amelioration of cognitive deficits and neurodegeneration.[9–11]

Hydrophobic drugs delivered orally encounter permeability problems and hence poor bioavailability. They undergo chemical and enzymatic degradation in the gastrointestinal tract and show extensive hepatic first-pass metabolism. Similarly, various additional factors hinder drug discovery and the development of an effective delivery of different therapeutic molecules for the treatment and prevention of AD. The inability to deliver drugs effectively to the brain is due to the numerous protective natural barriers surrounding the central nervous system (CNS) such as the blood–brain barrier (BBB). These natural barriers also limit the effectiveness of various potential drug-delivery systems (DDS) based on transdermal, buccal, and intravenous routes.[12,13]

Many strategies that include development of DDS, magnetic drug targeting, and drug carrier systems such as antibodies, liposomes, or nanoparticles (NPs) have been developed to overcome these problems. Among the various DDS, polymeric NPs have attracted great attention as potential DDS for the CNS because they can efficiently deliver a wide range of therapeutic molecules to the targeting area. These NP carrier molecules also fulfill the criteria for controlled and site-specific delivery of a variety of hydrophilic, hydrophobic natural and synthetic drugs, proteins, vaccines, and biological macromolecules.[14,15]

Despite various added advantages, CNS drug-delivery strategies through the intranasal route have received relatively little attention. Intranasal drugs are transported along olfactory sensory neurons to yield significant concentrations in the cerebrospinal fluid (CSF) and olfactory bulb. Recent evidence of direct nose-to-brain transport and direct access to CSF of neuropeptides bypassing the bloodstream has been shown in human trials, despite the inherent difficulties of delivery.[16,17]

Intranasal delivery is noninvasive and essentially painless, does not require sterility regulations, and is readily administered by the patient or health professionals. DDS are designed to promote the localized therapeutic effect and minimize toxic side effects. This may be achieved by optimizing the amount and duration of the drug in the vicinity of the target cells while reducing the drug exposure to nontarget cells.[18]

Owing to the success of the intranasal DDS, especially for brain targeting, the present investigation aimed to formulate a nanoparticulate delivery system for TQ targeted to the brain through a nasal route to avoid first-pass metabolism and its distribution to a nontargeted site with sustained action. This may lead to a decrease in peripheral side effects. The mucoadhesive polymeric NPs of TQ that we developed are expected to offer many advantages over conventional nasal dosage forms, such as increased nasal residence and possibility of drug release at a slow and constant rate to the brain.[17,19,20]

As part of the development studies for TQ delivery into the brain, the objective of the present study was to simultaneously investigate the plasma pharmacokinetics and brain distribution profiles of the TQ-loaded NPs in Wistar rats after intravenous and intranasal administration and to assess whether there is a direct nose-to-brain transport pathway.

Materials and methods

CS with medium molecular weight and degree of deacetylation about 96% and sodium tripolyphosphate (TPP) was purchased from Sigma-Aldrich (St Louis, MO). Potassium dihydrogen phosphate, methanol, sodium hydroxide (NaOH), and 1-octanol were all purchased from SD Fine Chemicals, Ltd (Mumbai, India). Glacial acetic acid was purchased from IOL Chemical Ltd (Mumbai, India). Methanol high-pressure liquid chromatography (HPLC) grade, acetonitrile HPLC grade, and ammonia solution analytical reagent (AR) grade were also procured from SD Fine Chemicals, Ltd. A cellophane tube (mol wt cut-off: 12,000 Da, flat with 25 mm, diameter of 16 mm, capacity 60 mL/ft) was obtained from Sigma-Aldrich. All reagents were of analytical grade.

Preparation of chitosan NPs using ionic gelation method

CS NPs were prepared according to the ionic gelation process.[21,22] Placebo NPs were obtained upon dropwise

addition of TPP aqueous solution (2 mg/mL) to a CS solution (1.5 mg/mL) with continuous stirring at room temperature. The formation of NPs was a result of the ionic interaction between the positively charged amino groups of CS and negative groups of TPP. The ratio of CS/TPP was established according to the preliminary studies. TQ-loaded NPs were obtained according to the same procedure and the ratio of CS/TPP remained unchanged. A variable ratio of TQ was incorporated in the CS solution prior to the formation of NPs in order to investigate the effect of the initial TQ concentration on the NP characteristics and in vitro release profiles. NPs were collected by centrifugation (Remi, Delhi, India) at 15,000 rpm for 30 minutes at 4°C and the supernatant was discarded.

Loading capacity, entrapment efficiency, and process yields

Process yield (*Y*) of NPs with desired particle size range and polydispersity index (PDI) was calculated from the weight of dried NPs recovered (W_1) and the sum of the initial dry weight of starting materials (W_2) as free drug:

$$Y = \frac{W1}{W2} \times 100. \quad (1)$$

Similarly, the entrapment efficiency (EE) and loading capacity (LC) of NPs were determined by ultracentrifugation at 15,000 rpm, 4°C for 30 minutes. The amount of free TQ in the supernatant was measured by the reverse phase-HPLC method (water:methanol:2-propanol::50:45:5% [v:v]; 2 mL min^{-1}) at 254 nm reported previously.[23] The EE and LC of NPs were calculated by the following equations and all measurements were performed in triplicate (n = 3).

$$\%EE = \frac{\text{Total drug} - \text{Free drug}}{\text{Total drug}} \times 100 \quad (2)$$

$$\%LC = \frac{\text{Total drug} - \text{Free drug}}{\text{Nanoparticle weight}} \times 100 \quad (3)$$

Dynamic light scattering (DLS) measurements

The particle size, particle size distribution, PDI, and zeta potential were determined by Zetasizer Nano ZS (Malvern Instruments Ltd, Malvern, UK). The sample volume used for the analysis was kept constant (1 mL). The particles exhibit Brownian motion, which causes the intensity of light to scatter from particles, which is then detected as a change in intensity with suitable optics and a photo multiplier. All the data analyses were performed in automatic mode with triplicate measurement within each run. The instrument is well equipped with appropriate software for particle size analysis and PDI.

Differential scanning calorimetry (DSC) study

DSC analysis of pure TQ, pure CS, physical mixture (CS + TQ), and freeze-dried TQ-loaded CS NPs was carried out using a PerkinElmer DSC-7® (PerkinElmer, Inc., Waltham, MA) calibrated with indium. A 5 mg sample was placed onto a standard aluminum pan, crimped and heated from 20°C –350°C at a heating rate of 5°C/minute under continuous purging of nitrogen (20 mL/minute). An empty sealed pan was used as reference. All samples were run in triplicate.

X-ray diffractometry (XRD)

X-ray diffractometry was used to investigate the physical form (crystalline or amorphous) of drug dispersion within the matrix of the CS NPs. The XRD experiments were performed over the range 2θ from 5 to 50°C, using an XRD (PANalytical X'pert PRO; PANalytical, Almelo, The Netherlands), with Cu Kα radiation at a scanning speed of 5°/minute.

Transmission electron microscopy (TEM)

The surface morphology of the prepared NPs was determined using TEM. A drop of nanosuspension was placed on a paraffin sheet and a copper grid was placed on the sample and left for 1 minute to allow the NPs to adhere. The grid was placed on a drop of phosphotungstate for more than 5 seconds. The remaining solution was removed by absorbing the liquid with a piece of filter paper and samples were air dried. The samples were further examined by TEM (Morgagni 268D; FEI Company, Hillsboro, OR).

Scanning electron microscopy (SEM)

The surface texture of the optimized NPs was further confirmed by SEM (Zeiss EVO40; Carl Zeiss, Cambridge, UK). Samples were spread over a double-sided conductive tape fixed on to a metallic stud and coated under vacuum with gold in a Blazers SCD020 sputter coater unit (BAL-TEC GmbH, Witten, Germany) in an argon atmosphere at 50 mA for 100 seconds.

In vitro release modeling

The in vitro release profile of the TQ suspension and TQ-loaded CS NPs was performed using dialysis sacs (MWCO 12,000 g/mole; Sigma-Aldrich). Equivalent volume of drug-loaded CS-TQ NPs (TQ was 4.275 mg) was filled in cellulose membrane dialysis sacs and study was performed using dissolution apparatus 2 (Veego, Mumbai, India) containing 500

mL of PBS (pH 6.5) at 37°C ± 0.5°C. At predetermined time intervals, aliquots were withdrawn from the released medium and replaced with the phosphate buffer. The samples were analyzed in triplicate using reported HPLC. The data obtained from in vitro drug release were fitted to various release models (zero order, first order, Higuchi, and Korsemeyer Peppas) to understand the possible mechanism of drug release from the NPs.[24]

Ex vivo permeation studies on nasal mucosa

Fresh nasal tissues were carefully removed from the nasal cavities of goats obtained from the local slaughterhouse. Tissue samples were fixed in cells displaying a permeation area of 0.785 cm^2 (Logan Instrument Corporation, Piscataway, NJ). Twenty milliliters of phosphate-buffered saline (PBS; pH 7.4) maintained at 37°C was added to the receptor chamber. After a preincubation time of 20 minutes, pure drug solution and formulation equivalent to 5 mg of TQ was placed in the donor chamber (2 mL) in each case. At predetermined time points, 0.5 mL samples were withdrawn from the receptor chamber, replacing the sampled volume with PBS over a period of 24 hours. The withdrawn samples were passed through a membrane filter before analysis. Blank samples (without TQ) were run simultaneously throughout the experiment to check for any interference. The amount of permeated drug was determined using reverse-phase HPLC.

Radiolabeling protocol

The TQ solution and TQ-NP1 were radiolabeled using technetium (^{99m}Tc) by a direct labeling method.[17,25] One milliliter of the TQ solution and TQ-NP1 (5 mg/mL) was taken separately and stannous chloride dihydrate solution (100 mg in 100 mL of 0.10 N HCl) was added. The pH was adjusted to 7.0 ± 0.50 using 50 mM sodium bicarbonate solution. To the resultant mixture, 1 mL of sterile ^{99m}Tc-pertechnetate (75 to 400 MBq) was added gradually over a period of 1 minute with continuous mixing. The resultant mixture was incubated (30°C ± 0.5°C) for 30 minutes in an inert environment. The final volume was made up using isotonic (0.90% w/v) saline solution. The radiochemical purity of ^{99m}Tc-TQ solution (^{99m}Tc-labeled TQ) and ^{99m}Tc-TQ-NP1 (^{99m}Tc-labeled TQ-loaded CS NP) were determined by instant thin-layer chromatography (ITLC; Gelman Sciences, Inc, Ann Arbor, MI) using a previously optimized mobile phase consisting of acetone (100% v/v). The effect of incubation time, pH, and stannous chloride concentration on radiolabeling efficiency were studied to achieve optimum reaction conditions. The optimized radiolabeled formulations were assessed for in vitro stability in normal saline solution, rat plasma and in rat brain homogenate. Finally, the optimized stable radiolabeled formulations were used to study biodistribution in rats.

Biodistribution and pharmacokinetics

All experiments conducted on animals were approved by the animal ethical committee of Jamia Hamdard, New Delhi (Proposal no 635/173/CPCSEA for the purpose of control and supervision on animals and experiments). Male Wistar rats aged 5–6 months, weighing between 200–250 g (average weight 200 g), were selected for the study. Three rats were used for each formulation per time point (0.25, 0.5, 2, 4, 6, 24 hours). Prior to nasal administration of the formulations, the rats were anesthetized using chloral hydrate (400 mg/kg, intraperitoneally) and the formulations were instilled into the nostrils with the help of a micropipette (100 µL) attached to a low-density polyethylene tube (0.1 mm internal diameter). The radiolabeled complex of ^{99m}Tc-TQ (100 mCi/100 mL) containing 500 µg of TQ/25 µL (equivalent to 0.5 mg/200 g body weight) was administered intranasally in each nostril.[10,11,26] The rats were held by their backs in a slanted position during the intranasal administration of the formulations. The rats were sacrificed at predetermined time intervals (0.25, 0.5, 2, 4, 6, 24 hours) and blood was collected by cardiac puncture. Subsequently, different tissues/organs including the brain were dissected, washed twice using normal saline solution, made free from adhering tissue/fluid, and weighed. The radioactivity present in each tissue/organ was measured using a shielded well-type gamma scintillation counter. The radiopharmaceutical uptake per gram in each tissue/organ was calculated as a fraction of the administered dose.[17]

The pharmacokinetic parameters were derived from Figure 1(A–C) using Kinetica (version 4.10; Innaphase, Philadelphia, PA) and recorded in Table 1. To evaluate the nose-to-brain targeting of different formulations, two indices, ie, brain-targeting efficiency (% DTE) and brain drug-targeting potential (% DTP) were adopted as mentioned below:[25,27]

$$\mathrm{DTE\%} = \frac{\left(\mathrm{AUC_{brain}}/\mathrm{AUC_{blood}}\right)_{\mathrm{in}}}{\left(\mathrm{AUC_{brain}}/\mathrm{AUC_{blood}}\right)_{\mathrm{iv}}} \times 100 \qquad (4)$$

In order to more clearly define nose-to-brain direct transport, the brain drug direct transport percentage (DTP%), was derived from the equation given below:

$$\mathrm{DTP\%} = \frac{\left(\mathrm{B_{in}} - \mathrm{B_x}\right)}{\mathrm{B_{in}}} \times 100, \qquad (5)$$

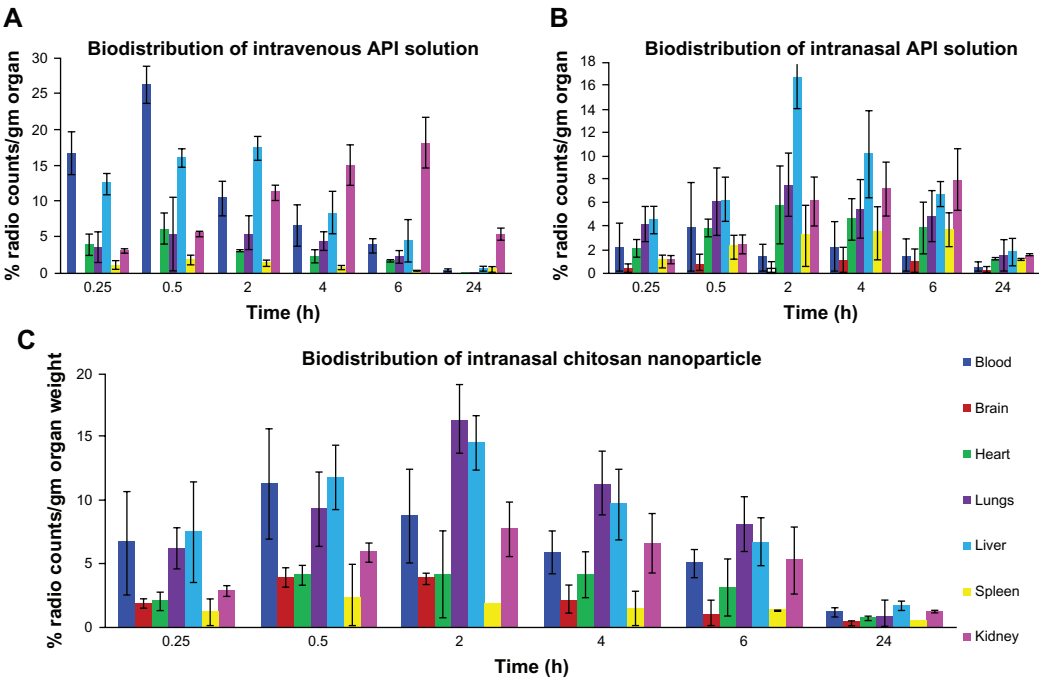

Figure 1 Biodistribution study of (**A**) TQ solution (intravenous), (**B**) TQ solution (intranasal), and (**C**) chitosan nanoparticles encapsulating TQ (intranasal).

where $B_x = (B_{iv}/P_{iv}) \times P_{in}$, B_x is the brain area-under-the-curve (AUC) fraction contributed by systemic circulation through the BBB following an intranasal administration; B_{iv} is the AUC_{0-24} (brain) following intravenous administration; P_{iv} is the AUC_{0-24} (blood) following intravenous administration; B_{in} is the AUC_{0-24} (brain) following intranasal administration; and P_{in} is the AUC_{0-24} (blood) following intranasal administration.

Statistical analysis

All data are reported as mean ± standard error of mean and the differences between the groups were tested using Student's *t*-test at a significance level of $P < 0.05$. More than two groups were compared using analysis of variance and the difference of $P < 0.05$ was considered significant.

Results and discussion

Formulation selection

Based on previously published literature, different trial compositions were performed to obtain an optimized formulation primarily on the basis of clarity and system aggregation (Table 2) and later with improved performance of minimum particle size and PDI, high process yield, EE, and LC (Table 3). High EE may be the consequence of an ionic interaction between negatively charged TQ with positively charged CS (Figure 2). Among various trials, the selected formulation S-3C (103.7 nm, 0.404, and 54.43%) had a smaller minimum particle, optimum PDI, and higher process yields than S-3A (368 nm, 0.215, and 44.86%) and S-3B (227 nm, 0.382, and 47.71%), respectively. Although S-4C, S-5C, and S-6B had a greater process

Table 1 Pharmacokinetic profile of different formulations

Formulations	Organ	C_{max} (count/g)	Tmax (hr)	$AUC_{0\rightarrow24}$	$AUC_{0\rightarrow inf}$	K_{el} (h^{-1})	$T_{1/2}$ (h)
TQ-NP 1 (intranasal)	Brain	2417.17	0.5	34074.377	41553.62	0.0696	12.62
	Blood	5453.73	0.5	57367.617	66666.795	0.0985	7.0355
TQ solution (intravenous)	Brain	242.88	2	2112.66	2309.37	0.1009	7.492
	Blood	30254.39	0.5	118220.82	121310.32	0.156	4.376
TQ solution (intranasal)	Brain	1717.74	2	2677.54	20318.97	0.0866	10.76
	Blood	4283.04	2	55383.78	69560.85	0.0929	9.489

Abbreviations: AUC_{0-24}, area under the curve; C_{max}, maximumconcentration; K_{el}, elimination rate constant; NP, nanoparticle; T_{max}, time at which concentration is maximum; TQ, thymoquinone.

Table 2 Results showing effects of different concentration of CS and TPP

Formulation code	Concentration of CS (mg/mL)	S no	Concentration of TPP (mg/mL)	Visual observation
S-1	0.5	A	1	Clear
		B	1.5	Clear
		C	2	Milky with aggregates
		D	3	Milky with aggregates
S-2	1.0	A	1	Clear
		B	1.5	Clear
		C	2	Aggregates
		D	3	Aggregates
S-3	1.5	A	1	Opalescent without ppt
		B	1.5	Opalescent without ppt
		C	2	Opalescent without ppt
		D	3	Milky with aggregates
S-4	1.75	A	1	Clear
		B	1.5	Opalescent with ppt
		C	2	Opalescent without ppt
		D	3	Milky with aggregates
S-5	2.0	A	1	Clear
		B	1.5	Clear
		C	2	Opalescent without ppt
		D	3	Aggregate
S-6	2.25	A	1	Clear
		B	1.5	Clear
		C	2	Opalescent without ppt
		D	3	Aggregate

Abbreviations: CS, chitosan; ptt, precipitate; TPP, tripolyphosphate.

yield than S-3C, the particle size was above 200 nm. Some formulations have low process yield whereas some have a higher yield due to low and high concentrations of CS, respectively. Therefore, S-3C was chosen as the optimized formulation of TQ-NPs. The above findings conclude that a unique ratio of CS:TPP (1.25–1.87) showed a particle size below 200 nm with a percentage yield greater than 25% whereas CS:TPP ratios exceeding the above limit showed a larger variability in particle size and percentage yield (Table 3). These findings are also in agreement with earlier reports that the ratio between CS and TPP is an important factor controlling the size distribution and process yield of NPs.[28] Although the minimum particle size obtained was 84.03 nm, containing 0.5 mg/mL CS and 1.5 mg/mL TPP (Figure 3), the low percent yield (18.78%) limits its applicability (Table 3). The mean particle size of optimized placebo NPs containing 1.5 mg/mL CS and 2 mg/mL TPP was found to be 103.6 nm. A comparative evaluation of particle size, PDI, and percentage yields of different preliminary formulations is listed in Table 3. On the basis

Table 3 Particle size and particle size distribution of placebo formulations

Formulation code	Concentration of CS (mg/mL)	Concentration of TPP (mg/mL)	Mean particle size (nm ± SD)	Mean (PDI ± SD)	Percent (yield ± SD)
S-1C	0.5	1	106.7 ± 8.0	0.395 ± 0.045	25.21 ± 2.30
S-1D	0.5	1.5	84.08 ± 8.03	0.587 ± 0.032	18.78 ± 3.46
S-2C	1	1	248.5 ± 5.6	0.253 ± 0.032	33.41 ± 5.13
S-2D	1	1.5	174 ± 4.0	0.333 ± 0.022	30.88 ± 2.24
S-3A	1.5	1	368.3 ± 6.6	0.215 ± 0.013	62.86 ± 3.56
S-3B	1.5	1.5	227.1 ± 9.2	0.382 ± 0.035	57.71 ± 2.50
S-3C	1.5	2	103.7 ± 8.02	0.404 ± 0.012	54.43 ± 3.12
S-4C	1.75	2	201.7 ± 7.6	0.595 ± 0.065	56.03 ± 3.09
S-5C	2	2	224.2 ± 8.6	0.623 ± 0.065	59.55 ± 2.37
S-6B	2.25	2	279.6 ± 5.8	0.537 ± 0.023	61.23 ± 3.25

Abbreviations: CS, chitosan; TPP, tripolyphosphate; PDI, polydispersity index; SD, standard deviation.

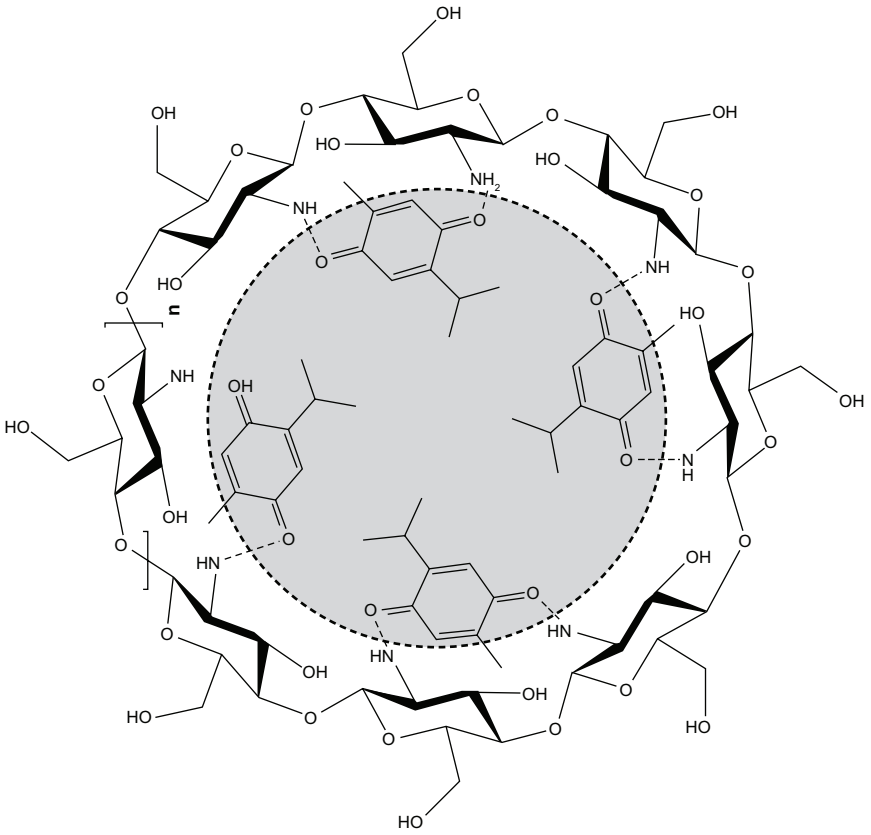

Figure 2 Chitosan nanoshell showing possible interaction between chitosan and thymoquinone.

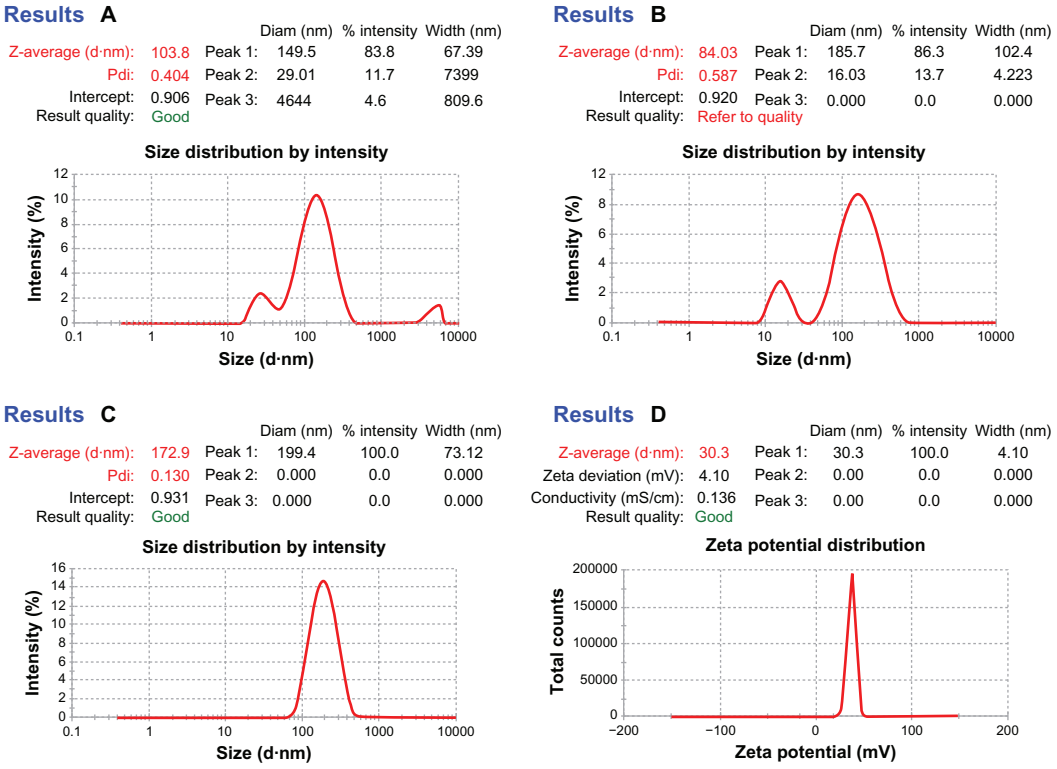

Figure 3 Dynamic light scattering technique for determining the particle size distribution of placebo nanoparticles (**A** and **B**) and TQ-encapsulated nanoparticles (**C**), and zeta potential of TQ-encapsulated nanoparticles (**D**).

Table 4 Particle size and particle size distribution of drug-loaded formulation

Code	Drug:polymer ratio	Concentration of CS (mg/mL)	Concentration of TPP (mg/mL)	Mean particle size (nm ± SD)	Mean zeta potential (mv ± SD)	Mean (PDI ± SD)	Percent (yield ± SD)
TQ-NP1	1:1	1.5	2	172.4 ± 7.4	30.3 ± 2.15	0.130 ± 0.065	53.42 ± 4.62
TQ-NP2	2:1	1.5	2	255.4 ± 5.6	27.6 ± 1.07	0.22 ± 0.045	47.82 ± 5.13
TQ-NP3	3:1	1.5	2	281.3 ± 4.7	24.5 ± 3.18	0.24 ± 0.064	42.12 ± 4.68

Abbreviations: TQ-NP, thymoquinone nanoparticles; CS, chitosan; TPP, tripolyphosphate; PDI, polydispersity index; SD, standard deviation.

of the above findings, S-3C was considered an optimized formulation.

The effects of drug concentration on particle size, PDI, EE, and LC of optimized TQ-NPs are summarized in Tables 4 and 5. It was observed that, upon increasing the drug: polymer ratio from 1 to 3, the average size of TQ-loaded NPs increased from 172.4 ± 7.4 (TQ-NP1) to 281.3 ± 4.7 nm (TQ-NP3). Increasing drug proportions in solution caused a reduction of CS and TPP interaction, which leads to an increased NP size. The increase in drug concentration also slightly increases the PDI value (0.24 [TQ-NP3] > 0.22 [TQ-NP2] > 0.130 [TQ-NP1]) with a decrease in percentage yield (42.12 [TQ-NP3] < 47.82 [TQ-NP2] < 53.42 [TQ-NP1]) (Table 4). The surface charge of optimized TQ-loaded NPs was found to be positive, indicating the partial stabilization of cationic charge of CS by anionic charged TPP.[22] The positive surface charge will also support better interactions with the negatively charged biomembrane.[29] This will be discussed in detail in the section on surface morphology.

LC and EE of TQ-loaded chitosan NPs

The EE and LC increased from 28.1% to 63.3% and 19.23% to 31.23%, respectively, depending upon the drug:polymer ratio (Table 5). The above data clearly shows that the 1:1 drug:polymer ratio shows better entrapment and LC. With the increase in initial CS concentration during the entrapment process, more protonized CS ($-NH_3^+$) were available in the system, as shown by increased surface charge, which leads to a stronger electrostatic attraction between TQ (negative charge) and CS (positive charge) (Figure 2). This high polymer concentration leads to an increase in binding sites for TPP with high EE. When the drug:polymer ratio increased, the ionic interaction between CS and TPP was hindered by drug molecules and hence led to lower entrapment and larger particle size (Tables 4 and 5). This finding seems to be in agreement with Mohanraj and Chen: the higher the drug concentration, the lower the entrapment and LC.[30]

Dynamic light scattering (DLS) measurements

Figure 3A and B show the particle size distribution of placebo-optimized CS NPs, whereas Figure 3C shows the TQ-loaded NPs. The size of the CS NPs could be influenced by factors such as TPP:CS ratio and concentration of CS. These trends show that the NP size was directly dependent on concentration and drug loading. The droplet size of the CS-based NPs was the smallest when the TQ:CS ratio was 1:1, whereas the droplet size was maximized by increasing the ratio to 3:1. Their droplet sizes at this concentration ratio were 172 and 281 nm, respectively (Table 4). The NPs showed a positive surface electric charge (measured by zeta potential), which varied depending on the proportion of CS and TQ (Figure 3D). Because of enough protonated amine groups remaining, the process of the ionic crosslinking occurs more easily for CS with a high degree of deacetylation. The data of mean particle size and zeta potential are listed in Table 4. The surface charge is the critical parameter on the stability of the nanosuspension and bioadhesion of particulate systems on biological surfaces. CS NPs are all positively charged, which is a typical characteristic of CS:TPP particles. This

Table 5 Effect of TQ concentration on EE and LC

Code	Volume of CS added (mL)	Volume of TPP added (mL)	Concentration of CS (mg/mL)	Concentration of TPP (mg/mL)	Concentration of drug added (mg)	Drug:polymer ratio	EE ± SD (%)	Percent LC ± SD
TQ-NP1	10	4	1.5	2	15.0	1:1	63.3 ± 3.5	31.23 ± 3.14
TQ-NP2	10	4	1.5	2	30.0	2:1	42.6 ± 4.2	26.67 ± 2.78
TQ-NP3	10	4	1.5	2	45.0	3:1	28.1 ± 3.8	19.23 ± 1.84

Abbreviations: TQ-NP, thymoquinone nanoparticles; CS, chitosan; TPP, tripolyphosphate; PDI, polydispersity index; SD, standard deviation; EE, entrapment efficiency; LC, loading capacity.

Table 6 Coefficient of correlation for optimized CS NPs

Release model	Equation	Coefficient of correlation (R^2)
Zero order	$Ct = Co + kt$	0.815
First order	$\log Ct = \log Co + kt/2.303$	0.964
Higuchi model	$Q = k\sqrt{t}$	0.981
Peppas model	$\log(M_t/M_\infty) = \log k + n \log t/2.303$	0.970
Release exponent (n)		$0.43 < n < 0.85$

Notes: Since the coefficient of correlation (R^2) for the Higuchi model was nearer to unity (ie, 0.981) for the TQ-loaded CS NPs, the best-fit model for TQ-loaded CS NPs was the Higuchi model.

Abbreviations: C_t, cumulative amount of drug release; C_o, initial amount of drug; k, release constant; CS, chitosan; M_t/M_∞, fraction of drug release; n, release exponent; NPs, nanoparticles; Q, fraction drug release; t, time; TQ, thymoquinone.

quality can be explained by the particle formation mechanism since the cationic charged amine groups are neutralized by their interaction with the anionic charge of TPP molecules. The residual amino groups are responsible for the positive potential.

A higher zeta potential in a certain range (24–30 mV) signifies the stability of CS NPs (Figure 3D and Table 4). It also signifies a hindrance imposed by long-chain amino groups and an anion adsorption to keep the high value of the electrical double layer thickness, thus preventing the aggregation. The zeta potentials in three batches of TQ-NPs are over +20 mV. The positive surface charge of NPs will improve the interaction, especially with the mucosal surfaces, which carry negative surface charge. This way, the biologically active molecule will act favorably on the target tissues.

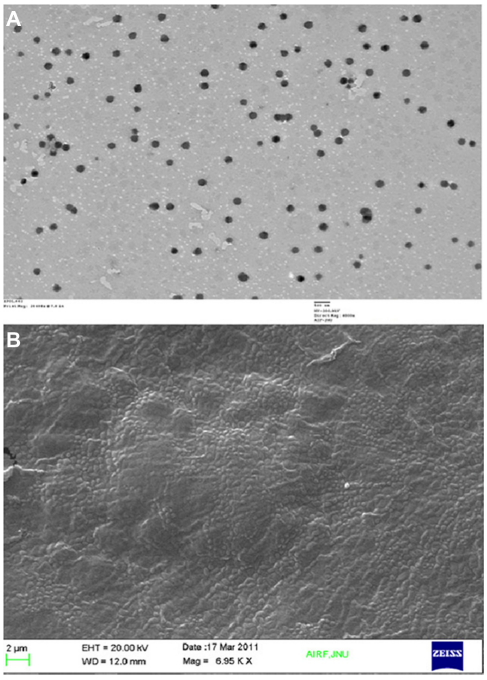

Figure 4 Transmission electron (**A**) and scanning electron (**B**) microscopy study of optimized nanoparticles.

Surface morphology (TEM and SEM study)

The shape and surface texture of the NPs could be detected using a number of sophisticated techniques such as TEM or SEM, respectively. NPs showed a round and smooth surface in TEM. The morphology of TQ-loaded CS-NPs as prepared is shown in Figure 4A and B. NP size was determined by TEM, which proved its sphericity. The particle size ranged between 150 and 200 nm (Figure 4A). The SEM of NPs proved their smooth surface texture (Figure 4B). Electron microscopy and DLS studies (Figure 3A–C) further corroborated the NP size.

Differential scanning calorimetry (DSC)

The DSC thermograms of TQ, physical mixture of TQ-CS, and CS- and TQ-encapsulated TQ-NPs, respectively, are shown in Figure 5A. An experimental study showed a sharp and well-defined endothermic peak at ~46.59°C equivalent to the melting point of TQ followed by an endothermic broad band at 146.7°C corresponding to the decomposition process, and ending at 160°C. Similarly, the physical mixture of TQ-CS showed the characteristic peaks of CS and TQ, which was absent in TQ-encapsulated CS NPs. Drug-loaded NPs showed a very small exothermic peak, whereas the polymer showed a predominant endothermic peak at 132.41°C, the drug had an endothermic peak at 126.053°C, and the physical mixture showed both drug and polymer peaks. No peak of TQ and CS was visible in the TQ-loaded NPs. This finding suggests that TQ is molecularly dispersed within the CS NPs showing the amorphous nature that further authenticates the entrapment of TQ.[28,31]

X-ray diffractometry (XRD)

In order to identify the physical state of the drugs incorporated in CS NPs, XRD was performed and the patterns of TQ, CS, and the physical admixture of TQ-CS as well as TQ encapsulated CS NPs are shown in Figure 5B(a–d). Powder diffraction data were collected at room temperature in the 2θ range 5.5° to 57.058° (d = 11.451–1.495 Å). Figure 5B represents the characteristic diffraction pattern of TQ at 6.7 Å. In the XRD patterns of the TQ-CS NPs, the characteristic peaks at $2\theta = 12.09°$, 18.65°, and 24.26° can be attributed to the crystalline structure of CS which is missing in TQ-encapsulated NPs (Figure 5B). TQ probably formed a

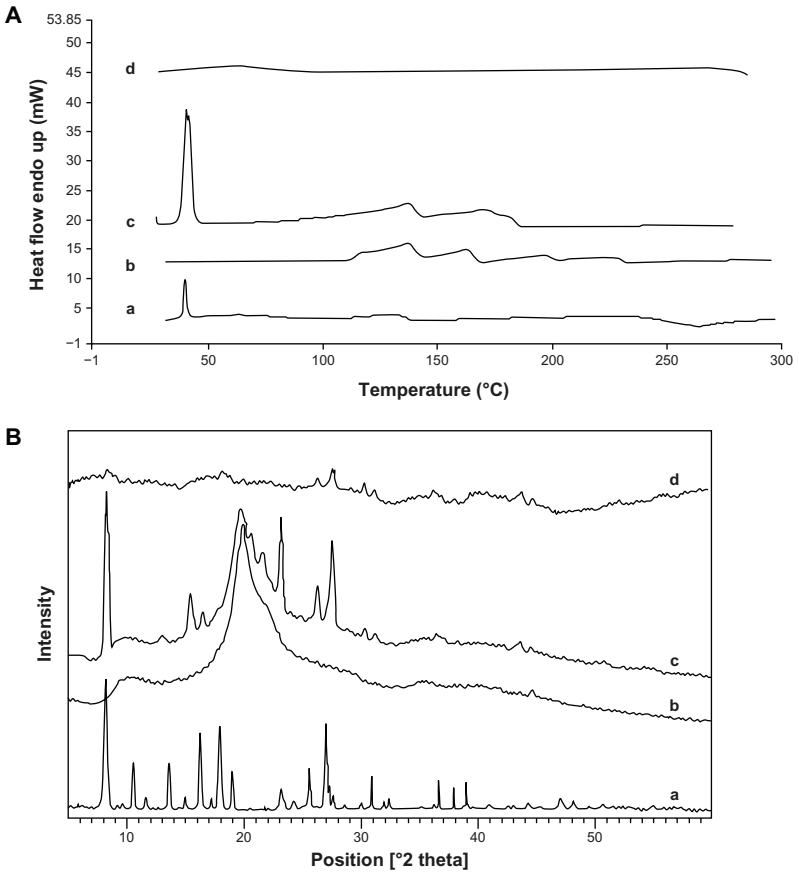

Figure 5 Differential scanning calorimetry (**A**) and X-ray diffraction spectroscopy (**B**) of thymoquinone (a), chitosan (b), physical mixture of thymoquinone–chitosan (c), and thymoquinone containing chitosan nanoparticles (d), respectively.

molecular dispersion or an amorphous nanodispersion within the CS matrix of the NPs.[32]

In vitro release modeling

The release profile of TQ from optimized CS NPs showed a sustained release pattern. It was observed that the released TQ primarily showed a rapid initial release (burst release) followed by a characteristic slow-release pattern. The initial rapid release of drug may be due to release of TQ from the NP surface, while at a later stage, TQ may be constantly released from the core of NPs as a consequence of CS

Table 7 In vitro radiolabeling stability in normal saline, rat plasma, and in rat brain homogenate

Sampling time (minutes)	Percentage of radiolabeling (retained)		
	Saline	Plasma	Brain homogenate
0.25	99.79 ± 2.6	97.57 ± 2.06	98.55 ± 2.96
0.5	99.74 ± 0.75	97.56 ± 3.12	98.68 ± 1.81
1	99.65 ± 1.95	97.45 ± 2.35	98.53 ± 2.12
2	99.43 ± 1.76	97.41 ± 2.76	97.48 ± 3.28
3	99.41 ± 2.61	97.31 ± 3.21	97.24 ± 2.77
4	99.34 ± 2.57	97.21 ± 3.43	97.42 ± 1.97
5	98.77 ± 4.3	96.84 ± 2.71	97.21 ± 3.32
6	98.74 ± 4.65	95.68 ± 4.05	96.79 ± 4.63
8	98.52 ± 4.02	95.46 ± 5.11	96.37 ± 1.01
22	97.47 ± 3.16	95.15 ± 5.16	96.25 ± 5.29
24	97.39 ± 4.26	95.07 ± 4.28	96.12 ± 3.52

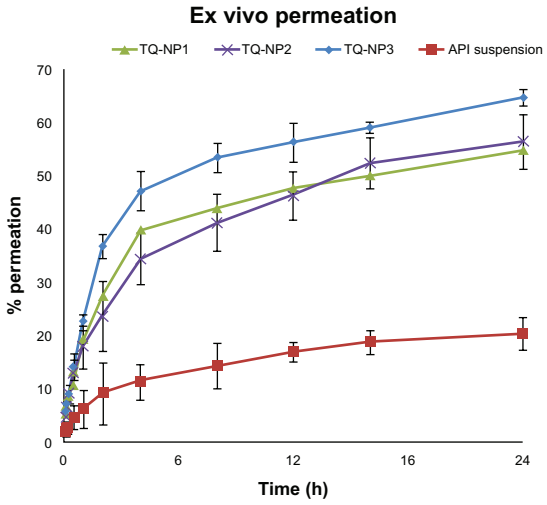

Figure 6 Ex vivo permeation of nanoparticles using porcine nasal mucosa.

hydration and swelling.[33] The release pattern was further confirmed by applying the release kinetic to ascertain the release order (Table 6). Among various models tried, the coefficient of correlation (R^2) for the Higuchi model was near to unity (ie, 0.981), therefore the best-fit model for TQ-NPs was the Higuchi model. When the release data were analyzed using the Korsmeyer–Peppas equation, the value of the release exponent n was between 0.43 and 0.85 (Table 6), which is an indication of both diffusion-controlled and swelling-controlled drug release, ie, anomalous transport.[33]

Ex vivo permeation studies on nasal mucosa

The TQ-loaded CS NPs showed more permeation compared to the pure drug solution (Figure 6). The significant difference in permeation profile ($P > 0.001$) of the optimized formulation TQ-NP1 might be due to the permeation-enhancing activity of CS. The maximum permeation in 24 hours was found to be >60% whereas API was only 20.39%. The increase in permeation of TQ could be attributed to an interaction of a positively charged amino group on the carbon two position of CS with negatively charged sites on the cell membranes. Similarly, one possible mechanism may be related to the tight junction permeability of the mucosal epithelial cells.[34] A justification for the least permeability of pure drug solution might be its hydrophobicity and possessing negative surface charge. Similarly, Richter and Keipert suggested that the drug should be lipophilic for better permeation through nasal mucosa.[35] The smaller size (<200 nm) and surface hydrophobicity of TQ-loaded CS NPs may support better partitioning through the biological membrane. Finally, on the basis of smaller particle size, higher percentage yield, better EE as well as LC, and relatively enhanced permeation profile, TQ-NP1 was selected as the final optimized formulation.

Radiolabeling stability study

TQ-NP1 effectively radiolabeled with ^{99m}Tc was optimized for maximum labeling efficiency and stability in normal saline, rat plasma, and in rat brain homogenate for 24 hours. The optimal $SnCl_2 \cdot 2H_2O$ concentration was found to be 100 mg/mL at pH 7.0 with an incubation time of 30 minutes. The radiolabeling stability achieved was 97.39 ± 4.26, 95.07 ± 4.28, and 96.12 ± 3.52 in normal saline, rat plasma, and rat brain homogenate, respectively (Table 7). The results suggested a high bonding strength and stability of ^{99m}Tc-TQ-NP1. Therefore, ^{99m}Tc-TQ-NP1 were found suitable for biodistribution studies in rats. The results obtained are also in agreement with the earlier findings.[17,25,27]

Biodistribution and pharmacokinetic study

The biodistribution pattern and different pharmacokinetic properties of intranasal administered NPs was evaluated using scintigraphic imaging. Scintigraphic imaging was performed using a gamma camera and the activity counts (TQ-TC^{99m}) in different organs such as brain, liver, kidney, spleen, heart, and lungs were performed with a gamma counter. Figure 1A–C shows the concentration of ^{99m}TC in different organs after the administration of intravenous ^{99m}TC-TQ solutions, intranasal ^{99m}TC-TQ solution, and intranasal ^{99m}TC-TQ-NP. The present investigation observed that the tissue concentration in the form of counts (^{99m}TC) was higher in the brain with the intranasal administration of TQ-NP in comparison to the TQ solution after intravenous and intranasal administration. The above finding might be due to existence of direct nose-to-brain transport bypassing the BBB.[36,37] Similar to systemic organs, the concentration of TQ-NP was higher in the brain compared to the TQ intranasal solution. This finding might be the combined upshot of the nanometric size range and mucoadhesive nature of the formulation. The special mucoadhesive property of CS will decrease mucociliary clearance, whereas the conventional intranasal formulation rapidly exits the nasal tract. The concentrations of ^{99m}TC-loaded TQ-NPs in the liver when administered intravenously was higher compared to intranasal ^{99m}TC-loaded TQ-NPs and ^{99m}TC solution because of the presence of the reticuloendothelial system (Figure 1). A similar pattern of ^{99m}TC-loaded TQ-NP distribution was also obtained in the lungs and in kidney.[17,25,27] The higher concentrations of ^{99m}TC achieved in the highly perfused organs, such as liver, lungs, and kidney are probably due to the combined activity of the circulating blood passing through the organs as well as particle uptake by reticuloendothelial system cells. The above results further support the

Table 8 Nose-to-brain drug-targeting parameters of different formulations

Formulations	Brain-targeting efficiency (DTE%)	Direct nose-to-brain transport (DTP%)	Relative bioavailability
TQ-NP 1 (intranasal)	3318.24 ± 65.79	96.99 ± 3.64	16.13 ± 0.87
TQ solution (intranasal)	206.94 ± 18.73	53.57 ± 8.34	1.26 ± 0.079
TQ-NP 1 (intravenous)	0.0179 ± 0.0023	–	–

Abbreviations: NP, nanoparticle; TQ, thymoquinone.

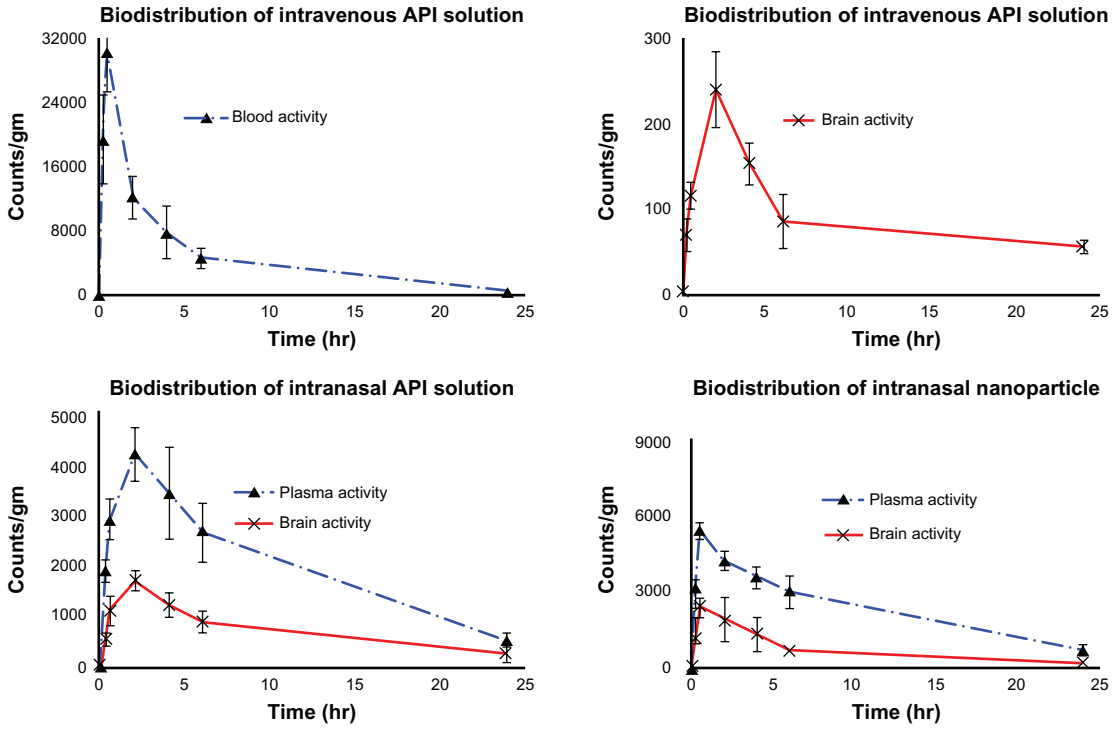

Figure 7 Concentration–time profile of thymoquinone (TQ) in plasma and brain after intravenous administration of TQ solution and intranasal administration of TQ solution and TQ nanoparticles, respectively (anti-clockwise).
Abbreviation: API, active pharmaceutical ingredient.

earlier finding by Wang et al after intranasal administration of CS NPs.[18,38]

The highest bioavailability in the brain might be the consequences of drug uptake from the nasal mucosa via three proposed pathways (Figure 1). One is the systemic pathway by which some of the drug is absorbed into the systemic circulation and subsequently reaches the brain by crossing the BBB. The others are the olfactory pathway and the trigeminal neural pathway by which partly the drug travels directly from the nasal cavity to the CSF and brain tissue.[39] We can conclude that the amount of drug reaching the brain tissue after intranasal administration is attributed to these three pathways.[20,40–42]

The pharmacokinetic parameters (Tables 1 and 8) were also calculated from a time-to-^{99m}TC-activity graph (Figure 7). Intranasal administration of TQ-NP1 showed lower T_{max} for brain (0.5 hours) compared to blood (2 hours). This may be attributed to preferential nose-to-brain transport following intranasal administration, which correlates with reports in the literature.[16,39–42] The brain:blood ratio of the drug was found to be higher for the TQ-NP1 formulation over the intranasal TQ solution (Table 1 and Figure 1). Similarly, the brain:blood ratio of the drug were higher for the intranasal TQ solution compared to the intravenous TQ solution. This finding further proved the significant role of the olfactory lobe in direct nose-to-brain transport. The concentrations of the drug in the brain following intranasal administration of TQ solution and TQ-NP1 were significantly higher ($P > 0.005$) at all sampling time points (24 hours) compared to the intravenous TQ solution. Moreover, following intranasal TQ-NP1, the drug concentrations in the brain were sustained for 2–3 hours, which was lacking in TQ solution (intranasal and intravenous). The substantially higher uptake in the brain after intranasal administration suggests a larger extent of selective transport of TQ-NP1 from nose-to brain. The formulations showed a significant difference in T_{max} (0.5 and 2 hours), C_{max} (242.88, 1717.74, and 2417.17 counts) and K_{el} (0.101, 0.086, and 0.0696 counts/hour) for intravenous TQ solution, intranasal TQ solution, and intranasal TQ-NP1, respectively. Significantly lower C_{max} ($P > 0.01$) and AUC ($P > 0.005$) for the intranasal TQ solution may be due to the mucociliary clearance under normal circumstances, which rapidly clears the instilled formulation. On the other hand, TQ-NP1 which shares an intrinsic mucoadhesive property showed a significant improvement in C_{max} and AUC. This demonstrates the value of the mucoadhesive agent in prolonging the contact time of the formulation with the nasal mucosa. The significantly higher AUC and C_{max} for TQ-NP1 compared to the TQ solution is attributed to the importance of nanoparticulate carriers.

Similarly, different nose-to-brain targeting parameters (Table 8) were calculated with the help of pharmacokinetics

parameters as shown in Table 1. DTP (%) represents the percentage of drug directly transported to the brain via the olfactory pathway and the trigeminal neural pathway. The TQ-NP1 showed significantly high ($P > 0.001$) DTE (%) and DTP (%) values among all the other formulations. The almost 15-fold higher DTE (%) and twofold higher DTP (%) for TQ-NP1 compared to the intranasal TQ solution shows the benefit of the mucoadhesive formulation (Table 8). The higher DTE (%) and DTP (%) suggest that TQ-NP1 has better brain targeting efficiency mainly because of substantial and direct nose-to-brain transport. The possible mechanism may be that the cationic TQ-CS systems showed a higher targeting efficiency in brain, which is consistent with previous studies.[43,44] These findings are in congruence with the observations reported by Zhang et al, who also proved the potential role of nanocarriers in nose-to-brain targeting.[45]

Conclusion

In the present investigation, TQ-encapsulated CS NPs were prepared successfully. A physical evaluation and electron microscope screening supported the suitability for intranasal administration. The scintigraphic study in rats demonstrated that intranasal administration delivers TQ to the brain rapidly and more effectively than previous methods. The accumulation of TQ-NP1 formulation within interstitial spaces and transport of the drug to the brain may be due the nanometric size range and the stretching of tight junctions within the nasal mucosa. The finding also supported the formulation's CSF-penetrating potential. The studies suggest intranasal delivery of TQ to be a promising approach for brain targeting as well as in reducing the systemic exposure. However, benefit-to-risk ratio and clinical intricacies need to be established scientifically for its suitability in clinical practice in the management of Alzheimer symptoms.

Acknowledgments

The authors are grateful to University Grant Commission (UGC), Government of India for providing fellowship to Sanjar Alam. Authors are also thankful for the support provided by Advanced Instrumentation Research Facility (AIRF), Jawaharlal Nehru University, and Institute of Nuclear Medicine and Allied Sciences (INMAS), New Delhi in this research activity.

Disclosure

The authors report no conflicts of interest in or financial benefit from this work.

References

1. Francis PT, Palmer AM, Snape M, Wilcock GK. The cholinergic hypothesis of Alzheimer's disease: a review of progress. *J Neurol Neurosurg Psychiatry*. 1999;66:137–147.
2. Desgranges B, Baron JC, de la Sayette V, et al. The neural substrates of memory systems impairment in Alzheimer's disease: A PET study of resting brain glucose utilization. *Brain*. 1998;121:611–631.
3. Forstl H, Hentschel F, Sattel H, et al. Age-associated memory impairment and early Alzheimer's disease. *Drug Res*. 1995;45(1):394–397.
4. Kumar V, Durai NB, Jobe T. Pharmacologic management of Alzheimer's disease. *Clin Geriatr Med*. 1998;14(1):129–146.
5. McGeer PL, Schulzer M, McGeer EG. Arthritis and anti-inflammatory agents as possible protective factors for Alzheimer's disease: a review of 17 epidemiologic studies. *Neurology*. 1996;47:425–432.
6. Ishrat T, Hoda MN, Khan MB, et al. Amelioration of cognitive deficits and neurodegeneration by curcumin in rat model of sporadic dementia of Alzheimer's type (SDAT). *Eur Neuropsychopharmacol*. 2009;19:636–647.
7. Akhondzadeh S, Abbasi SH. Herbal medicine in the treatment of Alzheimer's disease. *Am J Alzheimers Dis Other Demen*. 2006;21(2): 113–118.
8. Howesa MR, Houghton PJ. Plants used in Chinese and Indian traditional medicine for improvement of memory and cognitive function. *Pharmacol Biochem Behav*. 2003;75:513–527.
9. Al-Majed AA, Al-Omar FA, Nagi MN. Neuroprotective effects of thymoquinone against transient forebrain ischemia in the rat hippocampus. *Eur J Pharmacol*. 2006;543:40–47.
10. Al-Ghamdi MS. The anti-inflammatory, analgesic and antipyretic activity of *Nigella sativa*. *J Ethnopharmacol*. 2001;76:45–48.
11. Mansour MA, Nagi MN, El-Khatib AS, Al-Bekairi AM. Effects of thymoquinone on antioxidant enzyme activities, lipid peroxidation and DT-diaphorase in different tissues of mice: a possible mechanism of action. *Cell Biochem Funct*. 2002;20:143–151.
12. Lockman PR, Mumper RJ, Khan MA, Allen DD. Nanoparticle technology for drug delivery across blood–brain barrier. *Drug Dev Ind Pharm*. 2002;28:1–12.
13. Witt KA, Davis TP. CNS drug delivery: Opioid peptides and the blood-brain barrier. *AAPS J*. 2006;8(1):76–88.
14. Gabriel AS. Nanotechnology approaches for drug and small molecule delivery across the blood brain barrier. *Surg Neurol*. 2007;67:113–116.
15. Hans ML, Lowman AM. Biodegradable nanoparticles for drug delivery and targeting. *Curr Opin Solid State Mater Sci*. 2002;6(4):319–327.
16. Illum L. Transport of drugs from the nasal cavity to central nervous system. *Eur J Pharm Sci*. 2000;11:1–18.
17. Vyas TK, Shahiwala A, Marathe S, Misra A. Intranasal drug delivery for brain targeting. *Curr Drug Del*. 2005;2:164–175.
18. Wang X, Chi N, Tang X. Preparation of estradiol chitosan nanoparticles for improving nasal absorption and brain targeting. *Euro J Pharm Biopharm*. 2008;70:735–740.
19. Ugwoke MI, Verbeke N, Kinget R. The biopharmaceutical aspects of nasal mucoadhesive drug delivery. *J Pharm Pharmacol*. 2001;53: 3–21.
20. Fazil M, Md S, Haque S, et al. Development and evaluation of rivastigmine loaded chitosan nanoparticles for brain targeting. *Eur J Pharm Sci*. 2012;47(1):6–15.
21. Calvo P, Remunan-Lopez C, Vila-Jata JL, Alonso MJ. Chitosan and chitosan: ethylene oxide-propylene oxide block copolymer nanoparticles as novel carriers for proteins and vaccines. *Pharm Res*. 1997;14:1431–1436.
22. Aktas Y, Andrieux K, Alonso MJ, et al. Preparation and in vitro evaluation of chitosan nanoparticles containing a caspase inhibitor. *Int J Pharm*. 2005;298:378–383.
23. Ghosheh OA, Houdi AA, Crooks PA. High performance liquid chromatographic analysis of the pharmacologically active quinones and related compounds in the oil of the black seed (*Nigella sativa* L.). *J Pharm Biomed Anal*. 1999;19:757–762.

24. Ge H, Hu Y, Jiang X, et al. Preparation, characterization, and drug release behaviors of drug nimodipine-loaded poly(e-caprolactone)-poly(ethylene oxide)-poly(e-caprolactone) amphiphilic triblock copolymer micelles. *J Pharm Sci*. 2002;91:1463–1473.
25. Babbar AK, Singh AK, Goel HC, Chauhan UPS, Sharma RK. Evaluation of ^{99m}Tc labelled Photosan-3, a haematoporphyrin derivative, as a potential radiopharmaceutical for tumor scintigraphy. *Nucl Med Biol*. 2000;27:419–426.
26. Burits M, Bucar F. Antioxidant activity of *Nigella sativa* essential oil. *Phytother Res*. 2000;14(5):323–328.
27. Kumar M, Misra A, Babbar AK, Mishra AK, Mishra P, Pathak K. Intranasal nanoemulsion based brain targeting drug delivery system of risperidone. *Int J Pharm*. 2008;358:285–291.
28. Papadimitriou S, Bikiaris D, Avgoustakis K, Karavas E, Georgarakis M. Chitosan nanoparticles loaded with dorzolamide and pramipexole. *Carbohydr Polym*. 2008;73:44–54.
29. Quellec P, Gref R, Perrin L, et al. Protein entrapment within polyethylene glycol-coated nanospheres. I. Physicochemical characterization. *J Biomed Mater Res*. 1998;42:45–54.
30. Mohanraj VJ, Chen Y. Nanoparticles – A review. *Trop J Pharm Res*. 2006;5:561–573.
31. Joshi SA, Chavhan SS, Sawant KK. Rivastigmine-loaded PLGA and PBCA nanoparticles: Preparation, optimization, characterization, in vitro and pharmacodynamic studies. *Eur J Pharm Biopharm*. 2010;76:189–199.
32. Pagola S, Benavente A, Raschi A, Romano E, Molina MAA, Stephens PW. Crystal structure determination of thymoquinone by high-resolution X-ray powder diffraction. *AAPS PharmSciTech*. 2003;5(2):e28.
33. Ritger PL, Peppas NA. A simple equation for description of solute release II. Fickian and anomalous release from swellable devices. *J Control Release*. 1987;5:37–44.
34. Vllasaliu D, Exposito-Harris R, Heras A, et al. Tight junction modulation by chitosan nanoparticles: comparison with chitosan solution. *Int J Pharm*. 2010;400(1–2):183–193.
35. Richter T, Keipert S. In vitro permeation studies comparing bovine nasal mucosa, porcine cornea and artificial membrane: androstenedione in microemulsions and their components. *Eur J Pharm Biopharm*. 2004;58:137–143.
36. Tosi G, Costantino L, Rivasi F, et al. Targeting the central nervous system: In vivo experiments with peptide-derivatized nanoparticles loaded with Loperamide and Rhodamine-123. *J Control Release*. 2007;122:1–9.
37. Vergoni AV, Tosi G, Tacchi R, Vandelli MA, Bertolini A, Costantino L. Nanoparticles as drug delivery agents specific for CNS: in vivo biodistribution. *Nanomed Nanotech Biol Med*. 2009;5:369–377.
38. Wang X, He H, Leng W, Tang X. Evaluation of brain-targeting for the nasal delivery of estradiol by the microdialysis method. *Int J Pharm*. 2006;317:40–46.
39. Thorne RG, Pronk GJ, Padmanabhan V, Frey WH 2nd. Delivery of insulin-like growth factor-I to the rat brain and spinal cord along olfactory and trigeminal pathways following intranasal administration. *Neuroscience*. 2004;127:481–496.
40. Bhavna, Sharma V, Ali M, Baboota S, Ali J. Preparation and characterization of chitosan nanoparticles for nose to brain delivery of a cholinesterase inhibitor. *Ind J Pharm Sci*. 2007;69(5):712–723.
41. Al-Ghananeem AM, Saeed H, Florence R, Yokel RA, Malkawi AH. Intranasal drug delivery of didanosine-loaded chitosan nanoparticles for brain targeting; an attractive route against infections caused by AIDS viruses. *J Drug Target*. 2010;18(5):381–388.
42. Soni S, Kumar BA, Kumar SR, Banerjee T, Maitra A. Pharmacoscintigraphic evaluation of polysorbate 80-coated chitosan nanoparticles for brain targeting. *Am J Drug Del*. 2005;3(3):205–212.
43. Huo MR, Zhou JP, Wei Y, Lu L. Preparation of paclitaxel-loaded chitosan polymeric micelles and influence of surface charges on their tissue biodistribution in mice. *Acta Pharm Sin*. 2006;41:867–872.
44. Mahato RI, Kawabata K, Nomura T, Takakura Y, Hashida M. Physicochemical and pharmacokinetic characteristics of plasmid DNA/cationic liposome complexes. *J Pharm Sci*. 1995;84:1267–1271.
45. Zhang Q, Jiang X, Xiang W, Lu W, Su L, Shi Z. Preparation of nimodipine-loaded microemulsion for intranasal delivery and evaluation of the targeting efficiency to brain. *Int J Pharm*. 2004;275:85–96.